Journal of Photochemistry & Photobiology A: Chemistry 397 (2020) 112574

Contents lists available at ScienceDirect

Journal of Photochemistry & Photobiology A: Chemistry

journal homepage: www.elsevier.com/locate/jphotochem

Power-dependent nonlinear optical behaviours of ponceau BS chromophore at 532 nm via Z-scan technique

M.I. Rosli[a], M. Abdullah[b], G. Krishnan[a,c], S.W. Harun[d], M.S. Aziz[a,c,*]

[a] Department of Physics, Faculty of Science, Universiti Teknologi Malaysia, Johor Bahru, 81310, Johor, Malaysia
[b] Institute of Nano Optoelectronics Research and Technology (INOR), Universiti Sains Malaysia, 11800 USM, Penang, Malaysia
[c] Laser Center, Ibnu-Sina Institute for Scientific and Industrial Research (ISI-SIR), Universiti Teknologi, Malaysia
[d] Photonics Engineering Laboratory, Department of Electrical Engineering, Faculty of Engineering, Universiti Malaya, 50603 Kuala Lumpur, Malaysia

ARTICLE INFO

Keywords:
Nonlinear optics
Optical limiting
Ponceau BS dyes
Power-dependent
Z-scan

ABSTRACT

This paper reports on the power-dependent nonlinear optical (NLO) attributes for both nonlinear refractive index, n_2 and nonlinear absorption coefficient, β of Ponceau BS (PBS) chromophore, a synthetic organic compound that falls under azo family. Single-beam Z-scan technique was utilized for the nonlinear measurement. Dominant absorption peak is observed in the visible region due to the high conjugation of diazene functional group absorption. The existence of vital vibrational bonds e.g. the azo bond (1576 cm^{-1}) was confirmed via Fourier Transform Infrared Spectroscopy (FTIR). The intermolecular charge transfer (ICT) of delocalized electrons is responsible for the quick nonlinear response of the sample under intense laser excitation. Response from the closed and open aperture Z-scan technique indicates that PBS chromophore exhibits self-defocusing effects with negative sign of n_2 and reverse saturable absorption (RSA) in the order of 10^{-9} and 10^{-4} respectively. The real and imaginary components of third order susceptibility, χ^3 are relatively high in the order of 10^{-8} and 10^{-5} respectively under different laser powers (0.12, 0.14, 0.16, 0.18 & 0.20 W). In short, PBS chromophore shows promising features and can be considered as a potential candidate for various NLO applications under low-power laser operation.

1. Introduction

In the world of textile, dyeing industries and edible products, synthetic azo dyes have played a significant contribution on the production sector [1]. Azo dyes are organic molecules containing linkage of R_1-N = N-R_2 functional group, where R usually represents the aromatic hydrocarbons, the aryl group [2]. The type of Azo dyes, such as Acid Violet 7 [3], Bismarck Brown Y [4], Janus Green B [5], Methyl Red [6], Orange B [7], Poceau S [8], Sudan Red [9], and Tartrazine [10] etc., have contributed plenty of benefits in distinct disciplines to date. In fact, Azo dyes impart around 60–70 % of the entire 10,000 different types of dyes existing globally thanks to high stability, wide range of colors, and low market price [1,11,12].

In parallel, technological demand has created the necessity to find novelty in various compounds with descent nonlinear optical (NLO) properties due to its potential applications in the field of optoelectronics and telecommunications, such as high harmonic generation in lasers [13], optical switching [14], deployed telecommunication cables [15], optoelectronic oscillators [16], and ultrafast photonics stability [17]. Due to this reason, numbers of material has been extensively investigated for their performance, in which organic dyes have caught much attention due to their dynamics optical and electronics behavior especially in 3rd order NLO properties. Compared to conventional nonlinear optical crystalline materials, organic materials have various strengths, such as good processability, ultrafast response time and superior chemical flexibility [18]. Specifically, Ponceau BS (PBS) chromophore is one of the Azo-type dye adequate to the demand mentioned.

PBS chromophore appears deep red, highly soluble in water and has melting point at 181.0–188.0 °C. The molecular structure of PBS is as shown in Fig. 1. It is often used for histology & cytology [19,20], biological metabolisme [21], histochemical [22], and organic photosensitizer [23]. PBS chromophore perceived as a potential candidate to be utilized as an organic NLO material. However, there is limited number of research with inadequate critical appraisal especially on the nonlinear refraction (NLR) and nonlinear absorption (NLA) responses from the compound of interest. Therefore, this current work reports the experimental findings of linear and 3rd order NLO properties of PBS dye including its optical limiting (OL) performance as demonstrated by

* Corresponding author at: Department of Physics, Faculty of Science, Universiti Teknologi Malaysia, Johor Bahru, 81310, Johor, Malaysia.
E-mail address: safwanaziz@utm.my (M.S. Aziz).

https://doi.org/10.1016/j.jphotochem.2020.112574
Received 9 February 2020; Received in revised form 29 March 2020; Accepted 13 April 2020
Available online 30 April 2020
1010-6030/

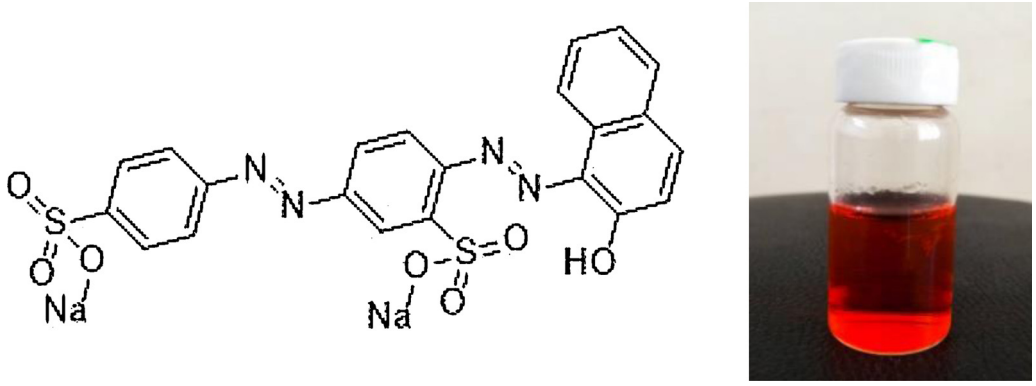

Fig. 1. The molecular structure of PBS composed of two functional groups of diazene $(NH)_2$ bonded in the compound. This functional group is responsible for the most reaction occurs in PBS.

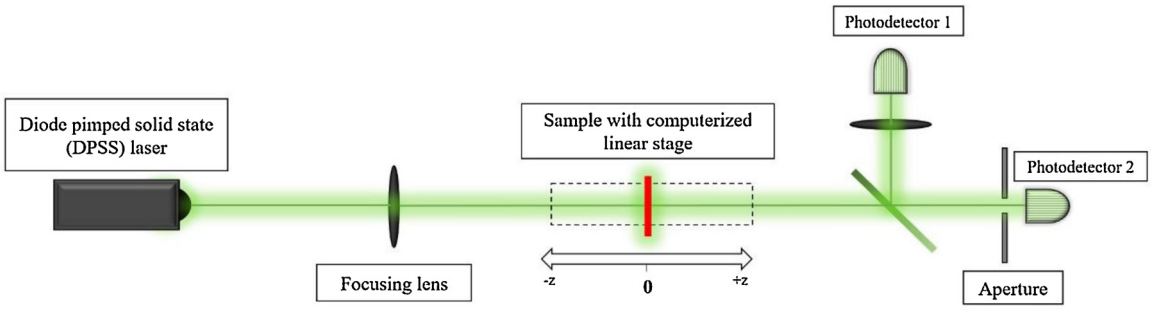

Fig. 2. Z-scan schematic diagram comprises of main DPSS excitation laser (532 nm). The irradiance was directly penetrating through the cuvette passing and 50:50 beamsplitter. Two photo-detectors (PD1 & PD2) were placed at different end of the Z scan set up. The far-field and the near-field of the irradiance were captured by PD1 and PD2 respectively.

Table 1
The lists of constant parameters of Z-scan measurement.

Parameters	Values
f	20 cm
r_o	0.19 cm
ω_o	0.0023 cm
L	0.1 cm

Table 2
The values of n_O (0.04 mM) and linear absorption coefficient at 532 nm.

Parameters	Value
n_O	1.3322
α (cm^{-1})	1.2708

single beam Z-scan technique using diode pumped solid state laser operating at 532 nm.

2. Experimental

2.1. Ponceau BS sample preparation

PBS with dye content ~60 % was purchased from Sigma-Aldrich and used without further purification. Stock solution of 0.5 mM was prepared for the experiment. The stock solution was then diluted with distilled water to achieve the concentration, C of 0.04 mM and used throughout the experiments. Fourier Transform Infrared Spectroscopy (FTIR) analysis was performed on the prepared sample by Perkin Elmer FT-IR /NIR Spectrometer to provide information on the basis of chemical composition of the sample.

2.2. Method

The linear refractive index, n_O, of PBS chromophore was measured by using Digital Hand-refractometer DR101-60 KRUSS, while the UV–vis linear absorption spectrum of PBS was measured by using Ocean Optics Maya 2000 Pro spectrometer. Values for both n_O and linear absorption coefficient α, were tabulated in Table 2.

A Z-scan technique was used in this study. It is a single beam technique to measure NLO properties, such as NLA, and NLR simultaneously as introduced by Sheik-Bahae [24,25]. This technique was employed due to its simplistic, accurate, efficient, and is highly sensitive method and is adequate to determine nonlinear refractive index, n_2 and nonlinear absorption coefficient, β [26–28]. However, Sheik-Bahae Model (SBM) does not accurately describing the nonlinear absorption associated with the variation of nonlinear refractive index in the presence of thermal contribution. Since this research was carried out via continuous-wave (CW), thus the thermal effect is dominant. As a result, Thermal Lens Model (TLM) was employed throughout the analysis. The authors one and all agree that TLM fit better to the experimental data than SBM for this specific setup. This was ensured by comparing the value of peak-valley separation to be greater than 1.7 z_r which prominently contributed by the effect of thermal.

Initially, the solvent (distilled water) was scanned through the Z-scan setup to check the existence of nonlinearity that could contribute towards the final reading. Finding shows that distilled water exhibits no significant nonlinearity under the range of utilized power. Then, the PBS chromophore was filled in a cuvette placed on the motorized stage at z-displacement and translated along the focus. The irradiance of the Gaussian laser beam changes when it converges and diverges, eventually adjusted the NLO transmittance [29]. The schematic diagram of Z-scan setup is depicted in Fig. 2.

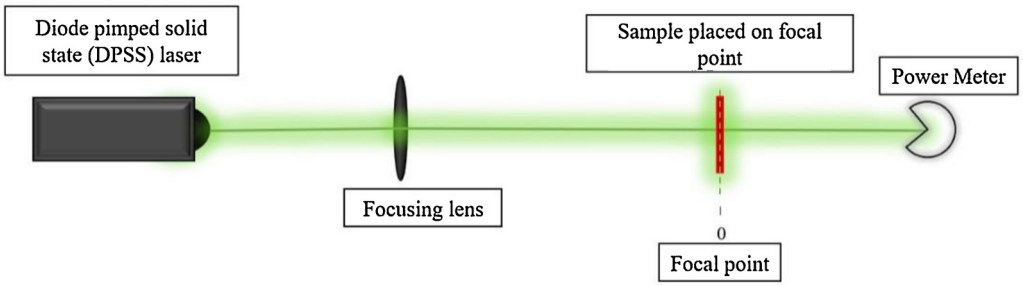

Fig. 3. The schematic diagram for performing OL measurement. Two photodetectors and beamsplitter were replaced by a digital power meters to measure the direct output power of transmitted irradiance.

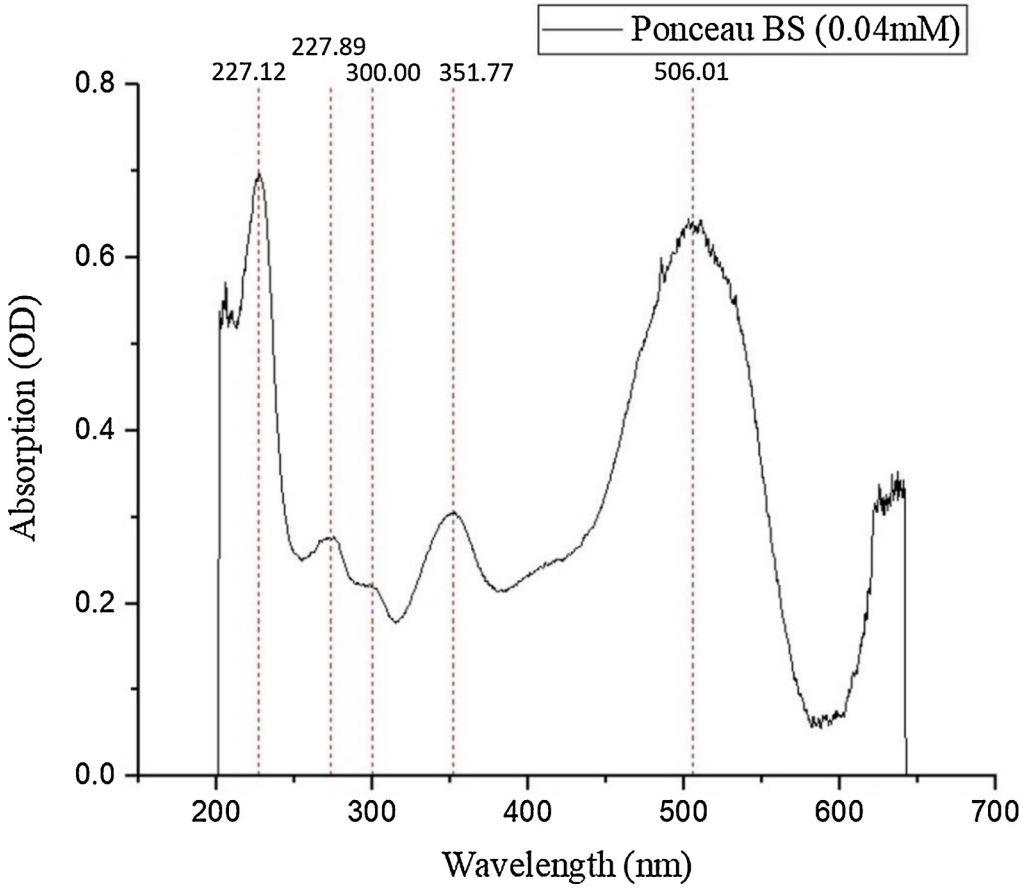

Fig. 4. The UV–vis spectral analysis of PBS chromophore.

In this setup, CW diode pumped solid state (DPSS) laser (Coherent Verdi-V5) operating at frequency doubled, λ = 532 nm was used as excitation laser. The output power of the laser can be tuned between 0.01 W to 5.00 W with high power stability of 1 %. The laser beam quality factor (M^2) and pointing stability of the laser are less than 1.1 and less than 2 μrad/ °C. These specifications are crucial for acquiring reliable Z-scan data. Two photodetectors (PD1 & PD2) (PDA 55 Thorlabs) were used to detect and measure the output transmittance of the signals. A positive lens (f = 20 cm) was utilized to focus the irradiance passing through the PBS chromophore. A quartz cuvette with path length L = 1 mm was used, lesser than the value of Rayleigh length at z_r= 3.12 mm, which is essentially vital precondition for Z-scan analysis of thin sample [30]. The cuvette containing the sample was placed on automated computerized linear stage (LTS-300, Thorlabs), and the cuvette was then translated along Z-displacement parallel to the laser transmittance axis. The signal detected by PD1 was recorded by an oscilloscope to scan the presence of NLA responses while the NLR response was detected by signals in PD2 respectively. The list of parameters used in the Z-scan set up was tabulated in Table 1.

The normalized transmittance from the near-field closed aperture as a function of θ is ruled by the following relation:

$$T_N^{TLM} = \left(1 + \theta \frac{2x}{1 + x^2}\right)^{-1} \quad (1)$$

where $\theta = \frac{2\pi L n_2 I_o}{\lambda \varepsilon_o c n_o} = \frac{\pi \alpha_o \omega_o^2 L}{2\lambda \kappa} \frac{\partial n}{\partial T} I_o$ denotes the on-axis phase shift, L denotes the sample thickness, I_o denotes the on-axis intensity at focus, ε_o denotes vacuum permittivity, c denotes the speed of light, ω_o denotes the Gaussian beam waist, κ denotes thermal conductivity, $\frac{\partial n}{\partial T}$ denotes the thermo-optics coefficient and, $x = \frac{z}{z_r}$, denotes dimensionless sample position.

On the other hand, the equation that governed the normalized transmittance from the far-field open aperture signal is given as below:

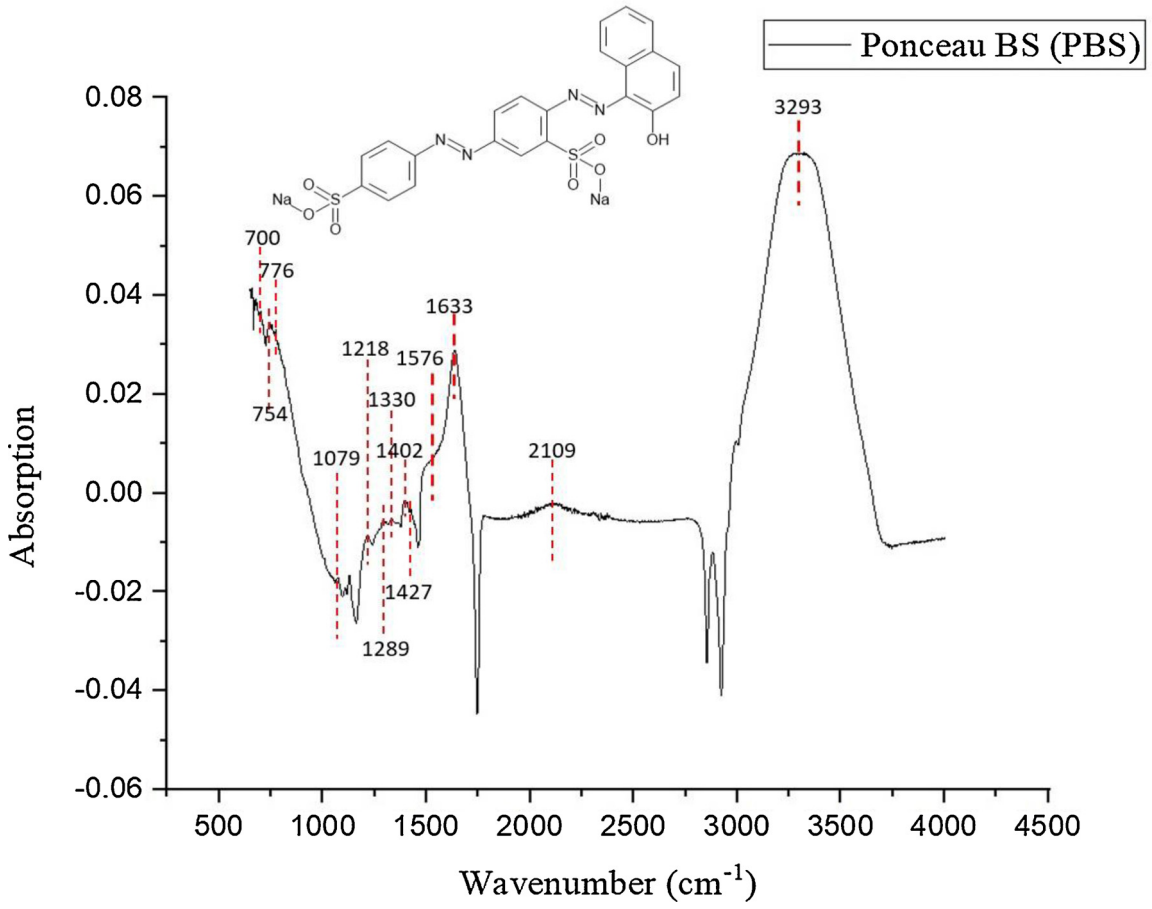

Fig. 5. FTIR spectrum of PBS chromophore.

Table 3
Summary of molecular vibration of PBS chromophore.

Wavenumber, ν (cm^{-1})	Group
700	C—H bending
754	C—H bending
776	C—H bending
1079	S═O stretching
1218	C—N stretching
1289	C—N stretching
1330	S═O stretching
1402	S═O stretching
1427	O—H bending
1576	N═N stretching
1633	C═C bending
2109	O—H bending
3293	O—H stretching

$$T_N = \sum_{m=0}^{\infty} \frac{(-\beta I_o L_{eff}/(1+x^2))^m}{(m+1)^{3/2}} \tag{2}$$

Where β is the nonlinear absorption coefficient and L_{eff} is the effective path length of the sample. The values of n_2 and β can therefore be obtained by fitting the experimental data with Eqs. (1) and (2) respectively. Thus, the real and imaginary parts of χ^3 were obtained from the following Eqs. (3) and (4) respectively.

$$RE\,\chi^3(esu) = 10^{-4}\frac{\varepsilon_o c^2 {n_o}^2}{\pi} n_2 \left(\frac{cm^2}{W}\right) \tag{3}$$

and

$$IM\,\chi^3(esu) = 10^{-2}\frac{\varepsilon_o c^2 {n_o}^2 \lambda}{4\pi^2}\beta\left(\frac{cm}{W}\right) \tag{4}$$

In order to ensure the NLA properties of the sample was due to the RSA induced ESA, the value of excited-state absorption cross-section, σ_{exc} were compared with the value of ground state coefficient σ_g. The σ_{exc} were obtained from normalized data fitting through open aperture, where

$$T = \frac{\ln\left(1+\frac{q_o}{1+x^2}\right)}{\frac{q_o}{1+x^2}} \tag{5}$$

that is the on-axis phase, $q_o = \frac{\sigma_{ESA}\alpha E_{L_{eff}}}{\hbar\omega_o^2 \pi\,\Omega}$, where E is the incident energy and Ω denotes as angular frequency. On the other hand, σ_g is rather a straightforward equation obtained from

$$\sigma_g = \frac{\alpha}{N_a C} \tag{6}$$

where, N_a is Avogadro constant.

Fig. 3 depicts the setup of OL where the cuvette was localized on the mounting stage. Concurrently, the PBS chromophore was placed on a fix position at the focal point of the utilized lens. The input power was gradually increased and monitored.

3. Results and discussion

The UV–vis absorption spectrum for PBS chromophore latter at hypsochromic shift is shown in Fig. 4. Four peaks were observed at 227.12, 272.89, 300, and 351.77 nm in UV region while a dominant peak was observed at 506.01 nm in visible region. It was observed that the absorption peaks in UV region were due to absorption of sodium benzene sulfonate and 2-naphthol molecules, whereas a dominant peak in visible region was due to absorption of diazene functional group

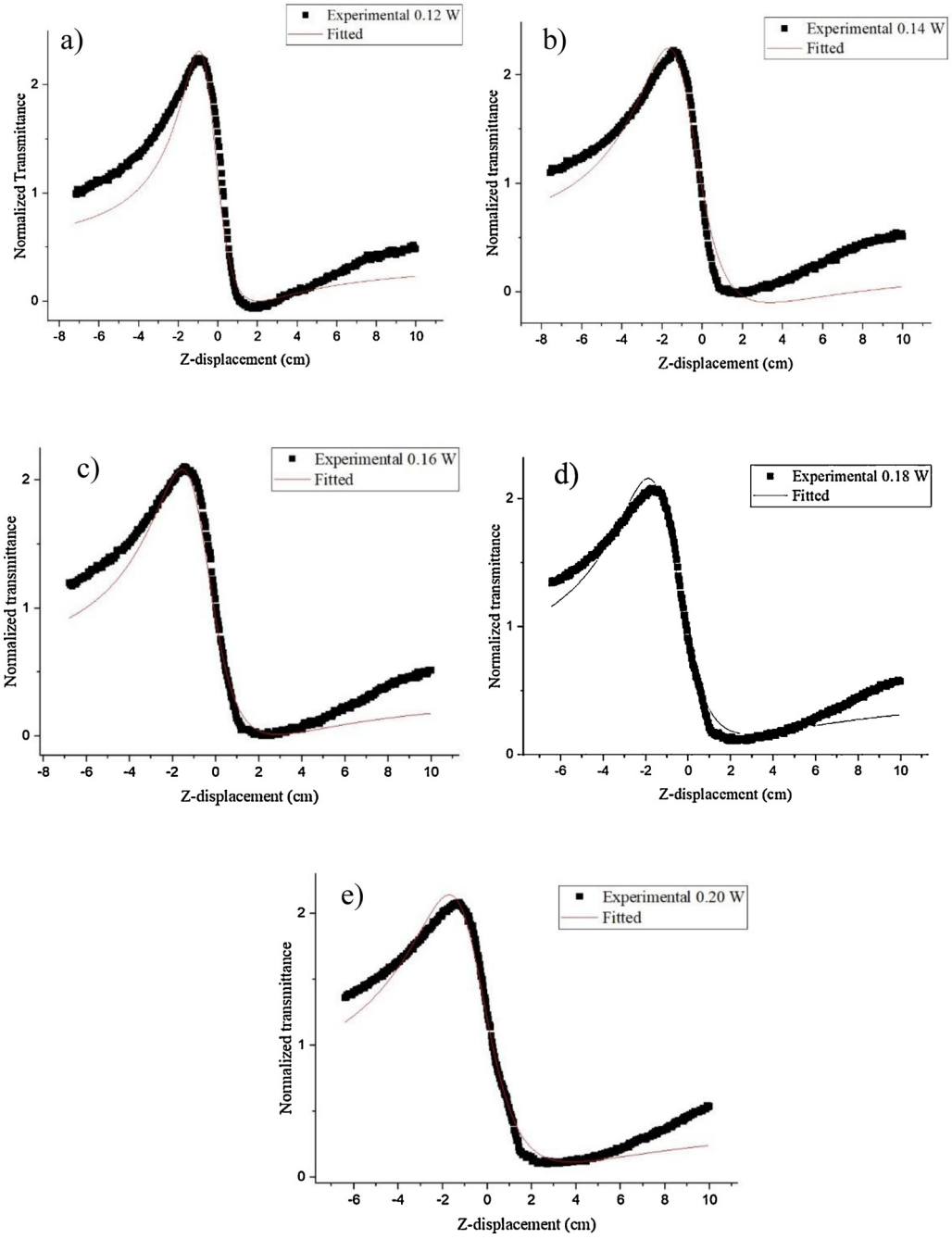

Fig. 6. Peak-valley closed aperture NLR response of PBS chromophore with laser polarization translated along the cuvette. The Z-scan set up is measured at different laser power: (a)0.12, (b)0.14, (c)0.16, (d)0.18, (e)0.20 W. The black dots indicate the experimental result lies on the red lines of theoretical fit curve.

Table 4
NLO attributes of PBS chromophore.

Power (W)	n_2 (10^{-9} cm^2W^{-1})	$RE\chi^3$ (10^{-8}esu)	β (10^{-4}cmW^{-1})	$IM\chi^3$ (10^{-5}esu)	$\lvert\chi^3\rvert$ (10^{-5}esu)	σ_{ESA} (10^{-19} cm^2)	R_o
0.12	−1.984	−8.962	12.251	2.420	2.420	7.102	13.46
0.14	−1.704	−7.701	9.614	1.899	1.899	14.194	26.90
0.16	−1.422	−6.425	9.191	1.816	1.816	27.543	52.20
0.18	−1.244	−5.623	8.293	1.638	1.638	49.843	94.47
0.20	−0.993	−.4.484	7.517	1.485	1.485	106.859	202.53

[31–33]. These bands are due to the vibrational effects of π-electrons transition ring currents in aromatic ring molecules existing in PBS chromophore [34]. Due to high conjugated double bond system in PBS molecule, the UV–vis absorption was shifted towards longer wavelength [35].

The FTIR analysis of PBS chromophore is shown in Fig. 5 in the range of 500 to 4000 cm^{-1} wavenumber. The peaks were assinged accordingly to the specific vibrational wavenumber, ν, from a standard

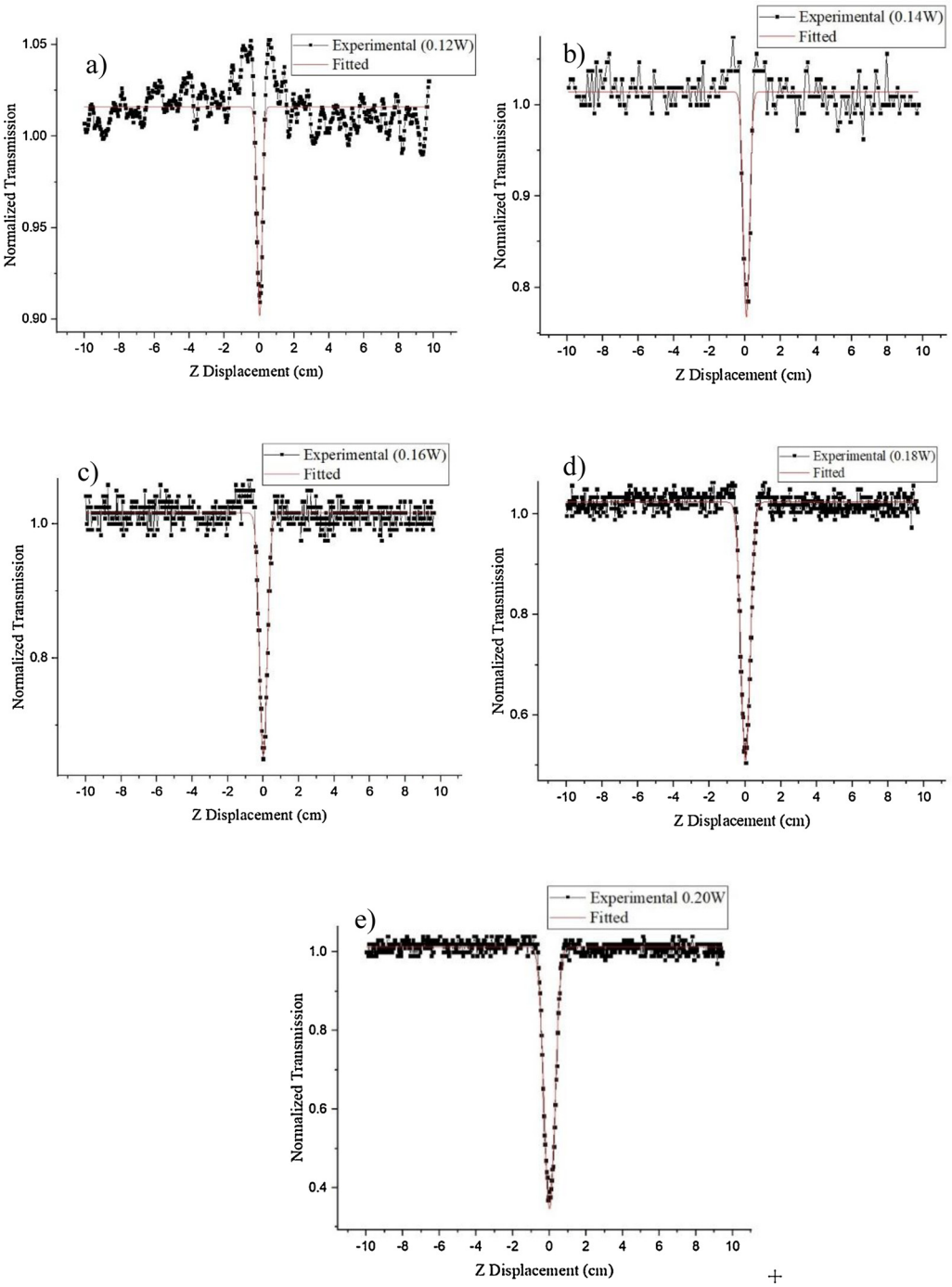

Fig. 7. The normalized transmittance of open aperture NLA response of PBS chromophore with laser polarization translated along the cuvette. The Z-scan set up is measured at different laser power: (a)0.12, (b)0.14, (c)0.16, (d)0.18, (e)0.20 W. The black dots indicate that experimental result lies on the red lines of theoretical fit curve.

IR Spectrum Table & Charts (Sigma-Aldrich). As observed, a dominant broad peak centered at 3293 cm^{-1} is due to the hydroxyl stretching vibrations. The main stretching vibration of diazene fuctional group existed at 1576 cm^{-1} as it was said to be geometrically isomerized as *trans*-Azobenzene [36]. There are three vibrations at 1402, 1330, and 1079 cm^{-1} due to S═O stretching, the sulfonate group (SO_3) as it is connected to the benzene ring. Furthermore, the C−N group is bonded to 2-naphthol molecule and produces stretching vibrations at 1289 and 1218 cm^{-1}. Then, the aromatic compund of C−H bendings vibrates at 700 (benzene derivatives), 754 (1,2,4-trisubstitute), and 776 (1,2-disubstitute), whereas the strong peak at 1633 cm^{-1} appeared due to C═C bending of aromatic rings.

The vibration of benzene rings and 2-naphthol compound contribute prominently in the FTIR spectrum. The vital components correlated to NLO attributes are the π conjugation system of C═C bending, N═N stretching, and free electron pair of sulfonate group. The intermolecular charge transfer of delocalized electron of π bonds from electron-donor-acceptor acts as catalyst to obtain an ultrafast response towards nonlinear optics. The summary of vibration groups for PBS chromophore is presented in Table 3.

As presented in Fig. 6, a series of Z-scan closed aperture NLR responses were obtained by varying laser powers. Consequently, the PBS

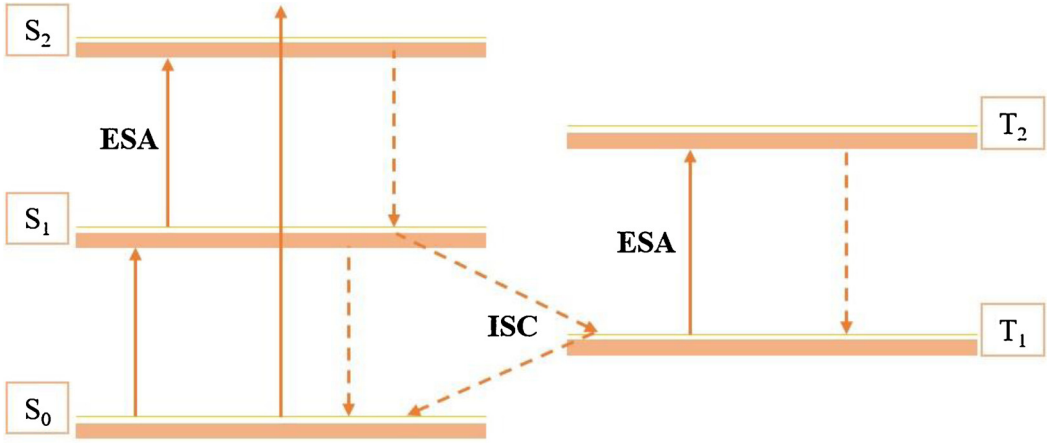

Fig. 8. The typical five energy levels comprise by singlet-singlet states (S) and triplet-triplet states (T). Solid lines represent radiative absorption whereas dashed line represent non-radiative transition.

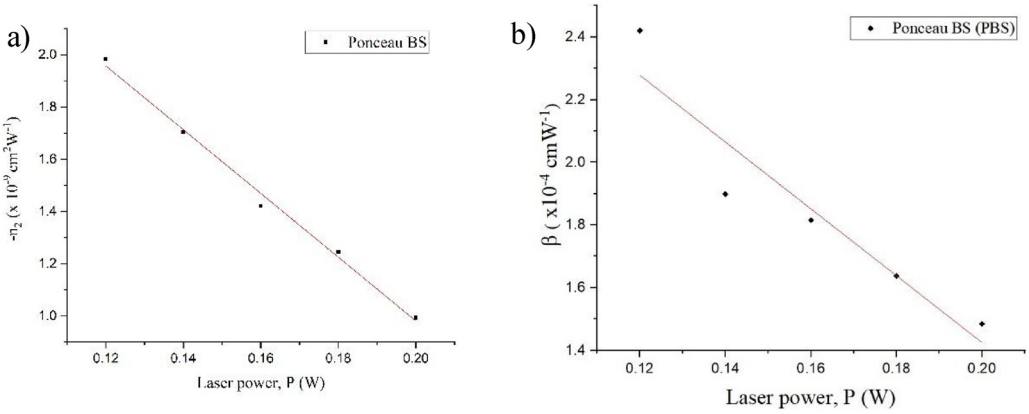

Fig. 9. (a) The value of n_2 against P (b)The values of β against P.

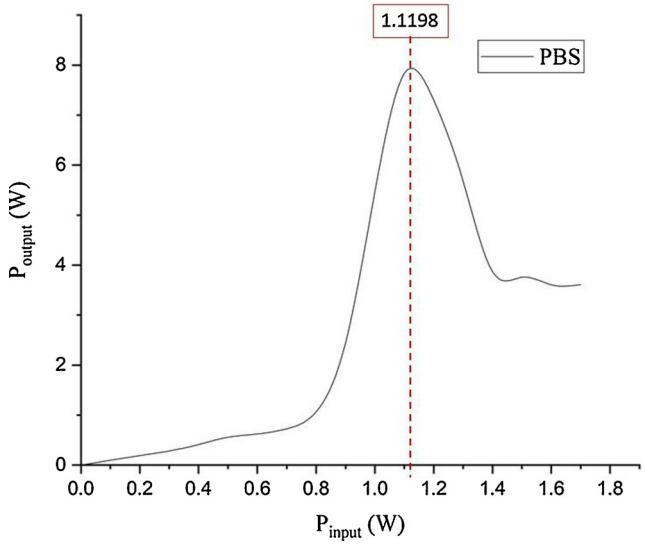

Fig. 10. The output signal taken during OL.

Table 5
The limiting threshold of PBS chromophore.

C (mM)	Limiting threshold (W)
0.04	1.1198

chromophore exhibits negative sign of NLR and self-defocusing effects due to the divergence of the irradiance. This effect is possibly ascribed as thermal lens effects (TLE), where the TLE appears caused by the absorption of localize irradiance propagation to the chromophore and created diffusion of spatial temperature profile isometrically over it. Under CW excitation, the excited state absorption (ESA) is assisted by the thermal effect. Plus, the result obtained highly related to the type of laser employed in the experiment which is CW laser. It is known that the thermal effects cannot be avoid due to dominant heat contribution under CW excitation

Then, as the samples were translated on the motorized stage, some of the absorbed energy was converted into heat and resulted in the changes in the refractive index. The vital part in this procedure lies in the Rayleigh region, in which the irradiance starts to defocus at a peak-point of the transmission. The chromophore reached a valley-point of the transmission at a particular point of focus. Thereafter, the laser beam gradually returned to its initial beam size. The value of n_2 was determine from the numerical fitting analysis. Eqs. (1) and (2) were used as primary guides to obtain the values of NLO attributes as tabulated in Table 4. The measured values within the range of 0.12 to 0.20 W laser power. According to Eqs. (1) and (2), where $I_o = \frac{P}{4\pi r^2}$, the relationship between P with n_2 and β are inversely proportional to each other thus, its numbers decrease by increasing power. Despite the thermal effects, the variation in the values of n_2 and β were assisted by interbond transition of two-photon absorption (TPA) [37–39]. As the compounds with the existence of aromatic rings increase the chances of electronic population within ICT π -bonds in the compound, especially for organic chromophores.

The open-aperture signals of PBS chromophore are shown in Fig. 7.

Analysis shows that the nonlinear absorption responses of the sample exhibit reverse saturable absorption (RSA) phenomenon, which is commonly reported in most of organic dyes [40,41]. The formation of RSA is indicated by the decrease in transmission of the sample at the focal ($z = 0$) with respect to increase input intensity As the power increases, the signal of RSA manifests dominant and stable output signals. The higher the irradiance, RSA are assisted by higher population of ESA as more energy are acquired to further photons excitation upon greater state. RSA process can only take place when the absorption of $\sigma_{ESA} > \sigma_g$, which is later confirmed by the calculation made based on the output transmission of the PBS sample. As plotted in Fig. 9, black dots resemble the obtained data through calculation whereas the straight red line specifies the regression of correlation strength between P with n_2 and β. The value of n_2, β, real, imaginary parts and magnitude of χ^3 were tabulated in Table 4. Here, according to Eqs. (3) and (4), it is investigated that $RE\ \chi^3$ and $IM\ \chi^3$ belong to n_2 and β respectively. At high value of $RE\ \chi^3$ it indicates the prominence NLR, whereas, at high value of $IM\ \chi^3$ it specifies superior NLA.

There are several transitions which possible for the mechanism of NLA phenomenon in PBS chromophore as elucidated in Fig. 8. It happened via (I) from the excitation of ground state, S_o to first excited state, S_1, then relaxes to T_1 via inter-system crossing (ISC), (II) Direct transition from S_0 to higher excitation state, S_n, which this transition is recognise as TPA, (III) Further excitation, S_n from S_1, this is known as ESA, (IV) from T_1 to T_n, is also known as ESA. Since the maximum value of β obtained from the experimental data through fitting at threshold power 0.12 W is greater than 0 ($\beta > 0$), it can be deduced that is PBS chromophore exhibits RSA. Consequently, the ESA assisted RSA were perceived at greater laser power. It was known that, with the employment of CW laser in this experiment which resulting the NLA properties are initiated from thermo-optics effects, finally enhance the ESA mechanism. Since the value of $\sigma_{ESA} > \sigma_g$ ($5.276 \times 10^{-20}\, cm^2$), it is satisfying the condition to conform the presence of RSA at open aperture measurement. Plus, the value rational value of PBS chromophore acquired between σ_{ESA} and σ_g were estimated in the order of 10^2 which later denoted as R_o. The high value of R_o indicates as best candidate to be utilized as OL.

The quantification OL are performed on a localized PBS chromophore at the focus, concurrently the input power was adjusted increasingly until it reaches saturation. The output power and limiting threshold of the chromophore were measured via digital power meter. Thus, the input against output power was plotted and procured as in Fig. 10. The presence of OL was caused by TPA phenomenon within the sample. However, it is well published where OL attributes arise through various principals such as NLA, ESA, nonlinear scattering (NLS), NLR etc. [42]. The contribution from NLA, NLR and ESA are confirmed due to the respond of Z-scan signals for both open and closed apertures. Contrarily, NLS mechanism is excluded due to its phenomenon originated from formation of microbubbles [43]. It was observed that, upon operating the experiment, the chromophore does not form any boils of microbubbles nor degraded. Thus, one and all agreed that the OL of PBS chromophore is contributed by NLR, NLA and ESA. Table 5 shows the limiting threshold of the samples. The limiting threshold tells a point of saturation which the OL start to arise. Commonly, the graph of OL is divided into three main regions which are linear region, active region and saturation region which represent a complete OL graph. The OL process possess by decreasing in the output signals as well as the transmittance when the irradiance captured and been absorbed by the molecules.

4. Conclusion

Overall, an aqueous PBS chromophore solution (0.04 mM) showed potential NLO properties under 532 nm laser excitation. It was confirmed that the existance of intermolecular charge transfer of delocalized electron of π bonds from C═C bending, N═N stretching and S═O stretching via FTIR analysis contribute to the NLO properties. The UV–vis spectrum shows dominant absorption peak at 227.12, 351.77 and 506.07 nm in which the latter occurred within the excitation domain. PBS chromophore affirmed to exhibits self-defocusing effects with negative sign of n_2 and RSA at open aperture. The fast response time of PBS chromophore has led to low threshold OL at 0.9037 W. The pleasing attributes of PBS chromophore could be further explored in advanced photonics and optoelectronics applications especially optical limiter for safety.

CRediT authorship contribution statement

M.I. Rosli: Experimental, Writing original draft, Formal analysis, Software.

M. Abdullah: Methodology, Conceptualization, Experimental set-up.

G. Krishnan: Investigation, Visualization, Data curation & validation.

S.W. Harun: Resources, Data fitting, Investigation & Optimization.

M.S. Aziz: Funding acquisition, Supervision, Project Administration, Reviewing & Editing.

Declaration of Competing Interest

The authors declare that they have no known competing financial interests or personal relationships that could have appeared to influence the work reported in this paper.

Acknowledgements

The authors would like to thank the Laser Centre, Ibnu-Sina Institute for Scientific and Industrial Research (ISI-SIR), Universiti Teknologi Malaysia for the support. This research work has been supported by UTM-Tier2 15J76 research grant.

References

[1] P. Sarwa, R. Vijayakumar, S.K. Verma, Adsorption of acid red 66 dye from aqueous solution by green microalgae Acutodesmus obliquus strain PSV2 isolated from an industrial polluted site, Open Access Lib. J. 1 (03) (2014) 1.
[2] J. Feng, T. M Heinze, H. Xu, C. E Cerniglia, H. Chen, Evidence for significantly enhancing reduction of Azo dyes in Escherichia coli by expressed cytoplasmic Azoreductase (AzoA) of Enterococcus faecalis, Protein Pept. Lett. 17 (5) (2010) 578–584.
[3] A.G. Shende, S.G. Ghugal, D. Vidyasagar, S.S. Umare, S.B. Kokane, R. Sasikala, Magnetically separable indium doped ZnSNiFe2O4 heterostructure photocatalyst for mineralization of acid violet 7 dye, Mater. Chem. Phys. 221 (2019) 483–492.
[4] J.J. Soriano, J. Mathieu-Denoncourt, G. Norman, S.R. de Solla, V.S. Langlois, Toxicity of the azo dyes Acid Red 97 and Bismarck Brown Y to Western clawed frog (Silurana tropicalis), Environ. Sci. Pollut. Res. - Int. 21 (5) (2014) 3582–3591.
[5] R. Zhang, Y. Zheng, Z. Liu, J. Chu, Usage of Janus green B for the improvement of the filling effect during replication process of nanoimprint nickel stamp, Micro Nano Lett. 13 (1) (2018) 24–26.
[6] J.K. Chen, S.M. Yang, B.H. Li, C.H. Lin, S. Lee, Fluorescence quenching investigation of methyl red adsorption on aluminum-based metal–organic frameworks, Langmuir 34 (4) (2018) 1441–1446.
[7] D. Tekin, T. Tekin, H. Kiziltas, Photocatalytic degradation kinetics of Orange G dye over ZnO and Ag/ZnO thin film catalysts, Sci. Rep. 9 (1) (2019) 1–7.
[8] S. Pandol, Statins Prevent Pancreatic Diseases Through Mitophagy Activation, Cedars-Sinai Medical Center Los Angeles United States, 2018.
[9] N. Abdollahi, M.Y. Masoomi, A. Morsali, P.C. Junk, J. Wang, Sonochemical synthesis and structural characterization of a new Zn (II) nanoplate metal–organic framework with removal efficiency of Sudan red and Congo red, Ultrason. Sonochem. 45 (2018) 50–56.
[10] D. Bhatt, K. Vyas, S. Singh, P.J. John, I. Soni, Tartrazine induced neurobiochemical alterations in rat brain sub-regions, Food Chem. Toxicol. 113 (2018) 322–327.
[11] R.G. Saratale, S.S. Gandhi, M.V. Purankar, M.B. Kurade, S.P. Govindwar, S.E. Oh, G.D. Saratale, Decolorization and detoxification of sulfonated azo dye CI Remazol Red and textile effluent by isolated Lysinibacillus sp. RGS, J. Biosci. Bioeng. 115 (6) (2013) 658–667.
[12] P.J. Wakelyn, Health and safety issues in cotton production and processing, Cotton, Woodhead Publishing, 2007, pp. 460–483.
[13] O. Neufeld, O. Cohen, Optical chirality in nonlinear optics: application to high harmonic generation, Phys. Rev. Lett. 120 (13) (2018) 133206.

[14] L. Wu, Z. Xie, L. Lu, J. Zhao, Y. Wang, X. Jiang, et al., Few-layer tin sulfide: a promising black-phosphorus-analogue 2D material with exceptionally large nonlinear optical response, high stability, and applications in all-optical switching and wavelength conversion, Adv. Opt. Mater. 6 (2) (2018) 1700985.
[15] Shiner, A. D., Reimer, M. A., O'sullivan, M., & Borowiec, A. (2018). U.S. Patent No. 9,960,843. Washington, DC: U.S. Patent and Trademark Office.
[16] J.H.T. Mbé, J.S. Kamaha, Y.K. Chembo, P. Woafo, Dynamics of wideband time-delayed optoelectronic oscillators with nonlinear filters, IEEE J. Quantum Electron. (2019).
[17] L. Lu, Z. Liang, L. Wu, Y. Chen, Y. Song, S.C. Dhanabalan, et al., Few-layer bismuthene: sonochemical exfoliation, nonlinear optics and applications for ultrafast photonics with enhanced stability, Laser Photon. Rev. 12 (1) (2018) 1700221.
[18] P. Chen, X. Yin, Y. Xie, S. Li, S. Luo, H. Zeng, et al., FTC-containing molecules: large second-order nonlinear optical performance and excellent thermal stability, and the key development of the "Isolation Chromophore" concept, J. Mater. Chem. C 4 (48) (2016) 11474–11481.
[19] R.C. Babb, D. Chandrasekaran, L.K. Zaugg, P.T. Sharpe, A mouse model to study reparative dentinogenesis, Odontogenesis, Humana Press, New York, NY, 2019, pp. 111–119.
[20] E.R. Molina, L.K. Chim, M.C. Salazar, G.L. Koons, B.A. Menegaz, A. Ruiz-Velasco, et al., A 3D tissue-engineered tumor model for Ewing's sarcoma that incorporates bone-like ECM and mineralization, ACS Biomater. Sci. Eng. (2019).
[21] R.L. Stingley, W. Zou, T.M. Heinze, H. Chen, C.E. Cerniglia, Metabolism of azo dyes by human skin microbiota, J. Med. Microbiol. 59 (Pt 1) (2010) 108.
[22] L. Rieppo, L. Janssen, K. Rahunen, P. Lehenkari, M.A. Finnilä, S. Saarakkala, Histochemical quantification of collagen content in articular cartilage, PLoS One 14 (11) (2019).
[23] S. Bose, K.R. Genwa, Fabrication of DSSCs with biebrich scarlet, alizarine cyanine green and evans blue dyes as new organic photosensitizers, Mater. Sci. 36 (4) (2018) 655–661.
[24] T. Xia, D.J. Hagan, M. Sheik-Bahae, E.W. Van Stryland, Eclipsing Z-scan measurement of λ/10 4 wave-front distortion, Opt. Lett. 19 (5) (1994) 317–319.
[25] M. Sheik-Bahae, A.A. Said, T.H. Wei, D.J. Hagan, E.W. Van Stryland, Sensitive measurement of optical nonlinearities using a single beam, IEEE J. Quantum Electron. 26 (4) (1990) 760–769.
[26] Y. Jia, Z. Li, M. Saeed, J. Tang, H. Cai, Y. Xiang, Kerr Nonlinearity in germanium selenide nanoflakes measured by Z-scan and spatial self-phase modulation techniques and its applications in all-optical information conversion, Opt. Express 27 (15) (2019) 20857–20873.
[27] E. Mathew, V.V. Salian, I.H. Joe, B. Narayana, Third-order nonlinear optical studies of two novel chalcone derivatives using Z-scan technique and DFT method, Opt. Laser Technol. 120 (2019) 105697.
[28] H. Li, Y. Li, J.Z. Huang, M. Liu, G. Zeng, Ultra-sensitive measurement of third-order optical nonlinearity via weak value amplification, Appl. Phys. Lett. 114 (16) (2019) 161906.
[29] L.F. Wu, Y.H. Wang, P.L. Li, X. Wu, M. Shang, Z.Z. Xiong, et al., Enhanced nonlinear optical behavior of graphene-CuO nanocomposites investigated by Z-scan technique, J. Alloys. Compd. 777 (2019) 759–766.
[30] M. Abdullah, H. Bakhtiar, G. Krishnan, M.S.A. Aziz, W.H. Danial, S. Islam, Transition from saturable absorption to reverse saturable absorption of carmoisine dye under low-powered continuous wave laser excitation, Opt. Laser Technol. 115 (2019) 97–103.
[31] H. Chen, B. Zheng, Y. Song, Comparison of PARAFAC and PARALIND in modeling three-way fluorescence data array with special linear dependences in three modes: a case study in 2-naphthol, J. Chemom. 25 (1) (2011) 20–27.
[32] M.E. Olya, A. Pirkarami, On the positive role of doping Cu and N 2 on TiO 2 in improving dye degradation efficiency: providing reaction mechanisms, Korean J. Chem. Eng. 32 (8) (2015) 1586–1597.
[33] Z. Zhang, Y. Deng, M. Shen, W. Han, Z. Chen, D. Xu, X. Ji, Investigation on rapid degradation of sodium dodecyl benzene sulfonate (SDBS) under microwave irradiation in the presence of modified activated carbon powder with ferreous sulfate, Desalination 249 (3) (2009) 1022–1029.
[34] C. Benhsinat, F. Beyoud, A. Wakrim, M. Azzi, A. Tazi, Decolorization and Degradation of Ponceau 4R by the Super-iron (VI) in an Aqueous Solution, (2017).
[35] D.L. Pavia, G.M. Lampman, G.S. Kriz, J.A. Vyvyan, Introduction to spectroscopy, Cram 101 Learning System, 4th edition, (2012).
[36] L.J. Bellamy, The Infrared Spectra of Complex Molecules: Volume Two Advances in Infrared Group Frequencies, Springer Science & Business Media, 2012.
[37] L. Moreira, R.F. Falci, H. Darabian, V. Anjos, M.J.V. Bell, L.R.P. Kassab, et al., The effect of excitation intensity variation and silver nanoparticle codoping on nonlinear optical properties of mixed tellurite and zinc oxide glass doped with Nd2O3 studied through ultrafast z-scan spectroscopy, Opt. Mater. 79 (2018) 397–402.
[38] A.S. Reyna, C.B. de Araújo, High-order optical nonlinearities in plasmonic nanocomposites—a review, Adv. Opt. Photonics 9 (4) (2017) 720–774.
[39] R.A. Ganeev, A.I. Ryasnyansky, A.L. Stepanov, T. Usmanov, Saturated absorption and nonlinear refraction of silicate glasses doped with silver nanoparticles at 532 nm, Opt. Quantum Electron. 36 (10) (2004) 949–960.
[40] S. Jeyaram, T. Geethakrishnan, Third-order nonlinear optical properties of acid green 25 dye by Z− scan method, Opt. Laser Technol. 89 (2017) 179–185.
[41] C. Babeela, M.A. Assiri, T.S. Girisun, Genuine two photon absorption and excited state absorption in Fe nanowires decorated β-BaB2O4 nanoplatelets, Opt. Mater. 95 (2019) 109267.
[42] D. Dini, M.J. Calvete, M. Hanack, Nonlinear optical materials for the smart filtering of optical radiation, Chem. Rev. 116 (22) (2016) 13043–13233.
[43] A. Wang, L. Cheng, W. Zhao, W. Zhu, D. Shang, Improved solubility and efficient optical limiting for methacrylate-co-porphyrins covalently functionalized single walled carbon nanotube nanohybrids, Dye. Pigment. 161 (2019) 155–161.